Brain Structure and Function
https://doi.org/10.1007/s00429-021-02387-5

ORIGINAL ARTICLE

The relationship between transcription and eccentricity in human V1

Jesse Gomez[1,2] · **Zonglei Zhen**[3,4] · **Kevin S. Weiner**[5,6]

Received: 6 January 2021 / Accepted: 24 August 2021

Abstract
Gene expression gradients radiating from regions of primary sensory cortices have recently been described and are thought to underlie the large-scale organization of the human cerebral cortex. However, the role of transcription in the functional layout of a single region within the adult brain has yet to be clarified, likely owing to the difficulty of identifying a brain region anatomically consistent enough across individuals with dense enough tissue sampling. Overcoming these hurdles in human primary visual cortex (V1), we show a relationship between differential gene expression and the cortical layout of eccentricity in human V1. Interestingly, these genes are unique from those previously identified that contribute to the positioning of cortical areas in the visual processing hierarchy. Enrichment analyses show that a subset of the identified genes encode for structures related to inhibitory interneurons, ion channels, as well as cellular projections, and are expressed more in foveal compared to peripheral portions of human V1. These findings predict that tissue density should be higher in foveal compared to peripheral V1. Using a histological pipeline, we validate this prediction using Nissl-stained sections of postmortem occipital cortex. We discuss these findings relative to previous studies in non-human primates, as well as in the context of an organizational pattern in which the adult human brain employs transcription gradients at multiple spatial scales: across the cerebral cortex, across areas within processing hierarchies, and within single cortical areas.

Keywords Transcription · Visual cortex · Eccentricity · V1 · Gene expression

Introduction

The contribution of gene transcription and tissue structures to the functional layout of the human cerebral cortex has become a major interest in systems neuroscience in the last decade (Jones et al. 2009; Krienen et al. 2016; Eickhoff et al. 2018; Huntenburg et al. 2018; Arnatkeviciute et al. 2019; Fornito et al. 2019; Fulcher 2019; Wei et al. 2019; Khrameeva et al. 2020; Seidlitz et al. 2020; Valk 2020). Recent research shows that active transcription of a small set of genes forms gradients across human cortex, which likely contribute to its regional differences in function and structure (Burt et al. 2018; Gomez et al. 2019). Specifically, a subset of genes increase or decrease their expression from primary to association cortices (Burt et al. 2018), likely also contributing to the hierarchical organization of functional processing streams (Gomez et al. 2019). The expression of some of these genes is correlated with macro- and microanatomical factors such as cortical thickness and myelination, respectively. Nevertheless, it is unknown if these transcription gradients also contribute to the layout of functional maps within individual cortical areas.

The relationship between transcription and the layout of functional maps within a single brain region remains unknown for two main reasons. First, the goals of previous studies were largely to examine the role of transcription in the parcellation of the brain into different anatomical and functional areas and thus, did not consider the unique topological layout of functional representations within areas

✉ Zonglei Zhen
zhenzonglei@bnu.edu.cn

1 Princeton Neuroscience Institute, Princeton University, Princeton, NJ, USA

2 Psychology Department, Princeton University, Princeton, NJ, USA

3 Beijing Key Laboratory of Applied Experimental Psychology, Beijing Normal University, Beijing, China

4 Faculty of Psychology, Beijing Normal University, Beijing, China

5 Helen Wills Neuroscience Institute, University of California Berkeley, Berkeley, CA, USA

6 Psychology Department, University of California Berkeley, Berkeley, CA, USA

Published online: 07 October 2021

(Jones et al. 2009; Krienen et al. 2016; Eickhoff et al. 2018; Huntenburg et al. 2018; Fornito et al. 2019; Khrameeva et al. 2020; Seidlitz et al. 2020; Valk 2020). Second, while there has been great interest in genetic expression and the development of single brain regions in previous research in non-human primates and mice (Watakabe et al. 2007; Watakabe 2009), this work largely focused on relating gene expression to the different layers within a single brain region, not the layout of the functional map along the two-dimensional cortical sheet. Filling in this gap in knowledge is important for linking transcription to human brain function at a finer spatial scale compared to these previous studies in humans - from areas and networks at the large-scale to functional maps within a single cortical area at the fine-scale. Accomplishing this with postmortem data would require a brain region with a functional representation that is anatomically predictable across individuals. Primary visual cortex (V1, also known as striate cortex) contains a well-characterized map of the retinal image that can be modeled in the absence of functional data (Wandell and Winawer 2011; Benson and Winawer 2018). While direct geniculostriate projections and a distinct transcriptional profile (Watakabe et al. 2007; Watakabe 2009) are unique features of V1 that will likely result in identified genes that may not fully generalize to other cortical regions, examining the relationship between transcription and eccentricity in human V1 will nonetheless be useful to test the ways in which gene expression may relate to functional and structural differences in a single region in human cortex.

Furthermore, understanding if/how functional representations are related to transcriptional differences across the cortical sheet in the adult brain can help the broad fields of cognitive neuroscience and human brain mapping understand the tissue structures that may ultimately give rise to different functional features of cortex, and relatedly, which genes may likely be impacted in deficits that alter such cortical functions. In order for such an experiment to be conducted, three hurdles have to be overcome. First, tissue samples have to be distributed with high enough density in a single cortical region to relate the differential gene expression of tissue samples with changes in the function of the underlying cortical sheet. Second, such a study would require a brain region with a large and anatomically consistent functional representation to accurately pool samples across donors. Third, a quantitative histological process capable of characterizing microarchitecture across the same piece of cortex would be required to relate potential transcriptional gradients with structural changes in the underlying cortical sheet. Here, we detail a protocol and experiment that achieves all three goals.

We employed a dataset (Hawrylycz 2012) detailing the transcriptomic landscape of adult human cortex from the Allen Human Brain Atlas (AHBA), which as described in a previous study (Gomez et al. 2019), densely samples the cortical tissue that comprises occipital and temporal visual cortex. Using tools from this previous work, tissue samples measuring the expression of over 20,000 genes from six donors were aligned to a common cortical surface, on which a functional map (eccentricity) of primary visual cortex was modeled. This empirical approach identified two sets of genes that were differentially expressed in posterior compared to anterior portions of human V1, in which the former is biased toward processing the more central portions of visual space, and the latter the far periphery of visual space. Furthermore, previously identified genes contributing to the organization of the visual processing hierarchy within occipito-temporal cortices more broadly are not correlated with the eccentricity map of V1. Enrichment analyses showed that a subset of the identified genes encode for cell populations related to inhibitory interneurons, synaptic structures, ion channels, as well as cellular projections. Interestingly, a majority of these genes have lower expression levels in the anterior compared to the posterior portion of V1, which predicts that the density of certain cell types and structures should be higher in foveal (posterior) compared to peripheral (anterior) V1. Using a histological pipeline, we validated this transcriptional prediction using Nissl-stained sections of postmortem occipital cortex.

Materials and methods

Postmortem tissue donor details

The following information has been collected by the Allen Institute for the Human Brain project, and can be found at https://human.brain-map.org/mri_viewers/data

Donor	Age (years)	Sex	Ethnicity	Postmortem interval (h)
H0351.2001	24	M	Black	23
H0351.2002	39	M	Black	10
H0351.1009	57	M	Caucasian	26
H0351.1012	31	M	Caucasian	17
H0351.1015	49	F	Hispanic	30
H0351.1016	55	M	Caucasian	18

AHBA tissue samples

The AHBA provides transcription data across the human brain, pooled from six donors and processed via microarray analyses. Specifically, microarray samples underwent strict normalization and data quality checks through AHBA as described here: http://human.brain-map.org. For data organization, preprocessing was identical to our previous

work (Gomez et al. 2019). Importantly, we follow the standardized processing pipeline proposed by Arnatkeviciute and colleagues (Arnatkeviciute et al. 2019). Briefly, the raw microarray expression data for each of the 6 donor brains included the expression level of 29,131 genes profiled via 58,692 microarray probes. We implemented six preprocessing steps. First, probes were excluded that did not have either (a) a gene symbol or (b) an Entrez ID. This resulted in 20,737 genes. Second, the expression profiles of all the probes targeting the same gene were averaged, and any gene that was not expressed significantly above background in at least 75% of relevant tissue samples (evaluated with a *t* test and having at least 2.6 standard deviations distance from background) were removed. Third, to remove variability in gene expression across donors, gene expression values of tissue samples were normalized by calculating z-scores separately for each donor. Fourth, because previous studies did not identify significant inter-hemispheric transcriptional differences, data from both hemispheres were combined. Fifth, only genes that are considered specific to brain tissue (Burt et al. 2018) and its relevant structures were analyzed to further minimize the number of comparisons and the likelihood of false alarms. Finally, mapping a tissue sample's genetic expression to an eccentricity value required aligning these tissue samples to a common cortical space. Each sample from the AHBA was associated with a 3D coordinate from the donor MRI brain volume and its corresponding coordinate (x, y, z) in MNI152 space. Each tissue sample was mapped to the nearest cortical surface vertex with a 5mm distance threshold and assigned to the visual field map in which that surface vertex was contained. Two tissue samples were excluded, which despite being mapped to peripheral V1, possessed atypical eccentricity values. This resulted in 54 tissue samples included in the analyses contributing to Fig. 1 and 52 tissue samples each probing 5,595 brain-specific genes in human V1 for the remaining analyses.

Defining the eccentricity map in human V1

Human visual areas are defined by two orthogonal functional maps: one of polar angle describing a receptive field's (RF) polar position along the circular image of the retina, and one of eccentricity, describing the RF's distance from the center of the visual field (the fovea). While maps of eccentricity are shared across early visual areas, the transition of one area to another is based on differences in polar angle (Wandell and Winawer 2011). Polar angle transitions between early visual areas occur with such regularity relative to the folding of the cerebral cortex that a model based on an individual's cortical anatomy is sufficient to automatically define areas V1 through V3 (Benson and Winawer 2018). We applied this model (Neuropythy) to a cortical surface of the MNI152 brain, which is an anatomical average of the human cerebral cortex from the Montreal Neurological Institute made from the average of 152 brains. This cortical space was chosen given that tissue samples from the donor brains of the AHBA have been aligned to the same MNI volumetric space. A cortical surface was produced for this anatomical volume using FreeSurfer (Dale et al. 1999). As described in the next section, we only use the eccentricity map produced from this atlas in the present study.

Testing if the expression of inter-regional (IRG) genes contribute to the cortical layout of the eccentricity map in human V1

In a previous study (Gomez et al. 2019), we identified 200 genes that formed opposed positive ("ascending") and negative ("descending") gradients along the visual processing hierarchy of occipito-temporal cortex. In the present study, we first tested if these inter-regional genes (IRG) identified previously also contributed to the layout of eccentricity within human V1. To do so, we performed Pearson correlations on the mean expression of these genes in the current tissue samples with eccentricity in V1 (Fig. 1). Beginning here, and onward, we restricted our analyses to only identify genes that may be related to the representation of eccentricity because the mapping of a tissue sample's coordinates to the cortical surface can be prone to error. For example, in volume space, a single tissue sample may overlap the upper lip and lower lip of the Calcarine Sulcus (CaS). However, the upper and lower lips of the CaS have different polar angle, but the same eccentricity, values. Thus, large mapping errors would result in the estimation of polar angle, but not eccentricity, values of a given tissue sample.

Comparing gene transcription and eccentricity in human V1

With tissue samples and eccentricity mapped to the same cortical surface, we extracted the underlying eccentricity from each tissue sample by taking the average of the vertices that were within a one-vertex radius of the vertex to which the tissue sample had been mapped via least Euclidean distance. As our previous study identified that genes distinguishing regions along a cortical processing hierarchy are organized into linear gradients of opposite sign (Gomez et al. 2019), we sought to test the *a priori* hypothesis that such gradients also exist in V1. However, given that we are performing analyses with tissue samples within a single brain region (rather than across regions, which can be separated by many centimeters of cortical distance), this analysis is particularly prone to being contaminated by the latent spatial autocorrelation that exists within gene expression of human cortex (Arnatkeviciute et al. 2019).

Consequently, to minimize the effect of spatial autocorrelation, rather than perform direct correlations between a tissue sample's eccentricity and the expression of a given gene, which is prone to false positives due to spatial autocorrelation, we take a contrastive approach. To do so, we first binned tissue samples into separate groups with an equal number (N=26) of tissue samples in posterior (biased more toward processing the central portion of visual space) and anterior (biased more toward processing the far periphery of visual space) portions of V1. The posterior region of interest (ROI) contained tissue samples within 0-17° of the eccentricity map in V1, while the more anterior ROI contained tissue samples >17° of the eccentricity map. This approach asks if there are any genes differentially expressed in posterior versus anterior samples of V1. Spatial autocorrelation, wherein neighboring cortical locations are genetically similar, would make observing a posterior-anterior difference in gene expression more difficult. This is preferable to the approach of correlating eccentricity and gene expression in V1, where spatial autocorrelation would likely induce many false positives, as it would be hard to disentangle distance and eccentricity (which are strongly correlated in V1). In this way, by testing which genes are differentially expressed in the posterior vs. anterior aspects of V1 using an ANOVA, we can link gene expression to underlying differences in functional representations (center vs. peripheral portions of visual space), while controlling for spatial autocorrelation as most tissue samples being compared are separated by several centimeters. To further reduce false positives, we restricted our analyses to only those genes considered to be specifically involved in processes associated with the central nervous system (brain-, neuron-, oligodendrocyte-, synaptome-, or layer-specific) as previously described (Burt et al. 2018). Similar to our previous approach (Gomez et al. 2019), an ANOVA was performed that contrasted expression level for each gene in tissue samples within posterior vs. anterior V1. The resulting p values were -log10 transformed and thresholded at a value of 2 (corresponding to p values <0.01) for further analyses. This approach resulted in 152 genes differentially expressed between posterior vs. anterior V1 (Table S1).

To quantitatively determine which genes were more highly expressed in the posterior vs. anterior portion of V1 (and vice versa), the top 152 differentially expressed genes were entered into an agglomerative clustering algorithm based on Euclidean distance [as done before (Gomez et al. 2019)], and genes were placed into one of two groups as determined by the highest clustering branch. A raster plot of the expression values for each gene clustered by group membership is shown in Fig. 2b, in which a clear "increasing" (lower expression in the central 0–17° of visual space compared to >17° of visual space) or "decreasing" (higher expression in the central 0–17° of visual space compared to >17° of visual space) expression pattern can be seen shared by genes within a given group. As a control analysis, we implemented a shuffling simulation (n=1000 shuffles) aimed to determine how many differentially expressed genes could be identified between posterior and anterior V1 solely as a result of noise inherent in these 52 tissue samples. To do so, half of the samples within posterior V1 and half of the samples within anterior V1 were randomly swapped into the other group. During each swap, a similar ANOVA approach was conducted for each gene and the number of genes that surpassed the same statistical threshold considered in our main analyses (p<0.01) were counted. Results of this simulation revealed that 93.2% of all shuffled permutations resulted in fewer (median n = 23) genes surviving significance than in our main analyses (n = 152). Furthermore, each time, the identified genes showed virtually no overlap with our 152 observed genes. The mean number of overlapping genes between the observed genes and a given shuffle was predominantly one or zero, with 0.68 genes overlapping on average. This analysis empirically supports that the posterior-anterior separation of equal groups of tissue samples in V1 implemented in our main approach identifies a stable set of genes that are differentially expressed in posterior compared to anterior portions of V1. To further examine the function of the identified genes, we performed enrichment analyses, as explained in the next section.

Gene enrichment analyses

The 152 identified genes were entered into an open-source enrichment analysis (ToppFun within the ToppGene Suite (Chen et al. 2009); https://toppgene.cchmc.org/enrichment.jsp), which detects if any functionally related genes exist within the identified set significantly higher than what would be expected by random chance (with significance values corrected using a Benjamini-Hochberg False Discovery Rate procedure). For determining if a particular gene group was significant, we chose a p value method of probability density function, and restricted our gene ontology identification to the following four categories: (i) GO: Molecular Function, (ii) GO: Biological Process, (iii) GO: Cellular Component, and (iv) TopCell Atlas: Human Adult Brain MTG. Importantly, choosing a different p value method (cumulative distribution function), did not significantly change the results. This approach produced five gene enrichment clusters belonging to the following ontology groups: cellular components (synapses, projections), molecular function (cation channels), or cell classes (inhibitory interneurons, macroglia). A subset of genes within each group are highlighted in Fig. 2b. The full list of genes belonging to each ontology group are in Table S2.

Quantifying histological slices of human cortex with *BrainWalker*

To further complement our enrichment analyses, we tested the hypothesis that gene transcription differences between functional representations within a single visual field map might induce microanatomical differences in the underlying cortical sheet, we developed a method to quantify human cytoarchitecture that (a) was repeatable across different histological samples, (b) could capture anatomical variation across cortical layers, and (c) was importantly, observer-independent. To achieve this goal, we developed an analysis pipeline called *BrainWalker* that quantifies the fraction of cell bodies and neuropil (cell-neuropil fraction, CNF) above background noise in a given histological stain. Importantly, this software slides or "walks" across cortical layers and columns, producing a vectorized description of the CNF for a desired piece of cortical ribbon. The software works as follows, and is illustrated in Fig. 3d. First, the user selects a ribbon of cortex to be quantified, tracing the middle of Layer 1 of cortex, and the corresponding length of the gray-white matter boundary (Fig. 3d, box 1). The two boundaries are then split into 200 equally spaced points. Points in Layer 1 and the white matter boundary are modeled as positive and negative electric charges, respectively, and then an electric field is modeled between the pial and white matter surfaces like a capacitor. Then, equipotential lines are drawn connecting each corresponding point on the two boundaries (Fig. 3d, arrow 1). These equipotential traversals are meant to model the shape of cortical columns traversing the cortical sheet, importantly fanning at gyral crowns (Smart and McSherry 1986). Each traversal is then split into 30 equally spaced points, and then a window slides between two neighboring traversals along these 30 bins (Fig. 3d, arrow 2). The underlying image (e.g., a Nissl stain) is thresholded twice, once at the mean pixel value, and then once more at 85% of the mean pixel value to further isolate the "peaks" or puncta associated with cell bodies and neuropil structures (Fig. 3d, arrow 3). While this threshold was somewhat arbitrary, a threshold was necessary to exclude irrelevant image structures such as holes from veins, tears in the tissue, or air bubbles on the mounting slide. These irrelevant values, or "background", where the white slide mount becomes visible can be seen as the large peaks in the histograms of Fig. S3. Fig. S3 also shows that the chosen threshold does not impact the interpretation of the findings: histograms of all pixel values from the foveal and peripheral slices indicate that foveal slices (red) have greater tissue content at the entire range of lower pixel values corresponding to cortical tissue all the way up to the mean pixel intensity (solid black line), which marks the beginning of brighter pixels representing the slide background. Differences between foveal and peripheral slices at these higher pixel intensities result simply from the cropping of the images; foveal slices had more of the underlying slide visible as the posterior slices of the occipital pole were smaller than more anterior slices. After this thresholding, at every bin, the CNF (fraction of pixels belonging to cell bodies and neuropil versus background) is quantified (Fig. 3d, arrow 4). The 30-bin vector for each traversal is then averaged across traversals, producing an average CNF contour detailing CNF from Layer 1 of cortex to white matter (Fig. 3d, arrow 5). In Fig. 3d, an example CNF contour is overlaid on a Nissl-stained section of human V1; one can appreciate how the peaks and valleys of the CNF contour highlight the different cell body densities across and between layers.

To generate CNF contours from human visual cortex, we used the freely available, high-resolution, Nissl-stained and Parvalbumin-stained coronal slices of human visual cortex from the Allen Institute's BrainSpan Atlas (http://www.brainspan.org/static/atlas). To compare foveal and peripheral cortex, within which genetic transcription is most differentiated in the present data and resulting anatomical differences are likely to be largest, we extracted slices (n=10) from the posterior CaS where foveal representations are located, and another ten slices from the anterior CaS where the peripheral representations are located. To ensure that differences in overall stain intensity would not bias results, and to mirror the normalization steps for the transcriptional data, each slice was normalized by the mean pixel value of all the neighboring white matter pixels. On a region of the cortical ribbon spanning 1.25 centimeters, we extracted the CNF of each slice from V1 and plotted the CNF of each slice in Fig. 3e comparing fovea and periphery for Nissl-stained cortex. We repeated this analysis with Parvalbumin-stained cortex (see Fig. 3e for bar plots). For Nissl stains, we computed a simple two-sample t test comparing the CNF between foveal V1 and peripheral V1 averaged across cortical layers (Fig. 3e). For the Parvalbumin stains, CNF varied by cortical layer, and t-tests were run comparing Layers 1–3 and Layers 4–6 separately (Fig. 3e). Parvalbumin was analyzed not only as an additional feature that could vary by eccentricity, but also as a control to ensure that foveal and peripheral cortical slices do not always vary by a global mean difference simply as a result of potential processing biases from the AHBA (differences in stain time, etc).

Statistical analysis

Statistical tests are described throughout the main text, and include one-way analyses of variance (ANOVA), two-tailed t tests, and Pearson correlations. The degrees of freedom are reported alongside each statistical test reported in the main

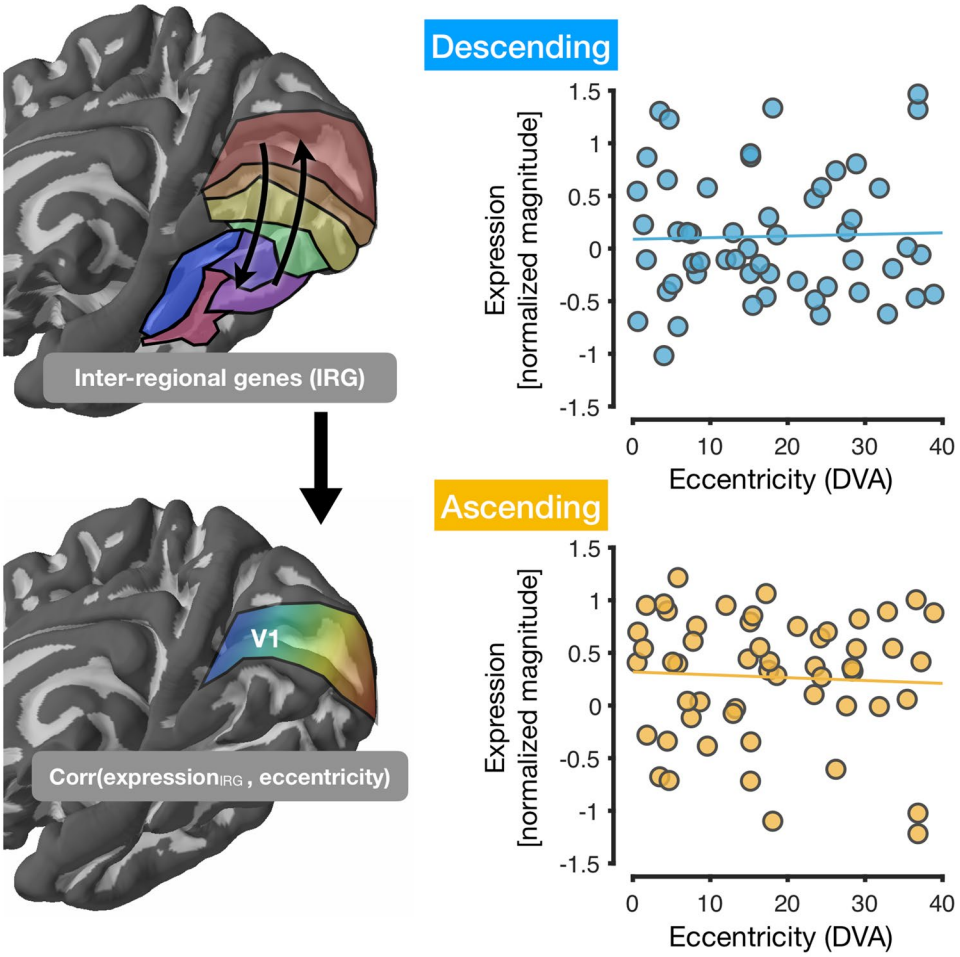

Fig. 1 Genes contributing to the position of cortical areas in the visual processing hierarchy are not correlated with eccentricity representation in V1. Within each tissue sample in human V1, average normalized expression was extracted for those genes within the ascending and descending expression gradients along the ventral visual processing hierarchy described before (Gomez et al. 2019; labelled inter-regional genes, or IRG, in the upper left). On the right, no significant correlations were found for the expression of IRGs (descending genes in blue; ascending genes in yellow) and the eccentricity of each tissue sample's location within V1 ($n = 54$, R^2's < 0.003, p's > 0.7). DVA: degrees of visual angle

text. The central mean and dispersion (standard error) for the *BrainWalker* analysis CNF values can be found in the figure legends. Statistical significance was set at $p < 0.05$ for all group comparisons or correlations. To avoid false positives during the gene selection process, we restricted our analysis to only genes expressed differentially at a significance level beyond p values of 0.01 (the top 2.7% of genes), similar to our previous approach (Gomez et al. 2019), and gene enrichment analyses were FDR corrected.

Results

To examine the relationship between transcription and eccentricity in human V1, we first identified tissue samples ($n = 52$) from the AHBA located within V1 by aligning all donor cortical hemispheres to a common space. In this common cortical space, we also employed the Neuropythy (Benson and Winawer 2018) toolbox to model both the borders and functional representations of primary visual cortex. In brief, V1 surrounds the Calcarine Sulcus (CaS) and its composite neurons (in this case, voxels) form a retinotopic map representing the image projected on the retina. This representation contains two orthogonal maps: eccentricity (distance from the central visual field) and polar angle (polar position around the visual field). Because these maps couple with the folding of cortex so tightly, they can be modeled from anatomy alone, which offers a promising opportunity to quantify how differential gene expression in the adult human brain may contribute to functional representations within a single cortical area. The present study focuses on eccentricity due to methodological issues when mapping tissue samples to polar angle representations-issues which do not affect the mapping between tissue samples and eccentricity representations (see Materials and methods).

After mapping each tissue sample to a cortical location within human V1, we then examined if genes identified previously that contribute to the hierarchical organization of the visual processing hierarchy [e.g., those genes that differentiate regions comprising the ventral and lateral occipitotemporal cortices as explored previously (Gomez et al. 2019), here termed inter-regional genes (IRGs)] are also genes that contribute to the layout of a functional map

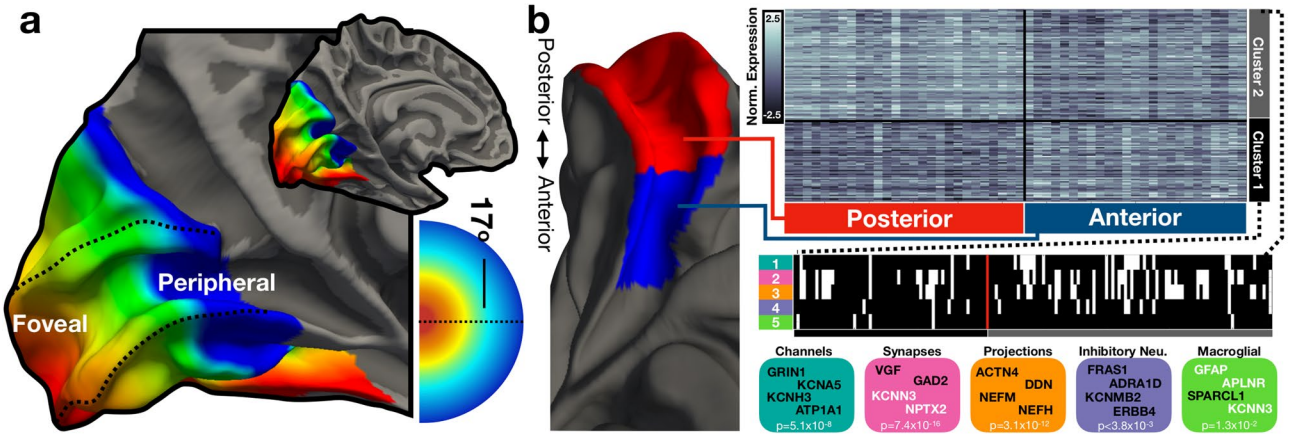

Fig. 2 Identifying genes with differential expression between posterior and anterior portions of V1. **a** Eccentricity representation from a probabilistic atlas (Benson and Winawer 2018) of visual cortex projected onto the Freesurfer (Fischl et al. 1999) average cortical surface. The boundaries of V1 are outlined with dotted black lines, and the colormap values are shown on the semicircle inset to the right. 17° is highlighted on the color wheel, as it was the cutoff value differentiating the posterior portion of V1 (<17°) from the anterior portion. **b** Left, the location of the posterior (red) or anterior (blue) ROIs used to group tissue samples overlaid on V1. Right, upper: raster plot depicting the expression of the 152 significant genes clustered by whether they have higher expression in posterior or anterior tissue samples. Right, lower: results from gene enrichment analyses showing the five categories of interest with white lines depicting a particular gene's membership to a given category. Black and gray rectangles to the right of the raster plot highlight each gene's membership to either Cluster 1 (higher expression in the anterior ROI) or Cluster 2 (higher expression in the posterior ROI). Example genes from each category are shown within colored boxes. Gene names written in black text show decreasing expression from the posterior to anterior portions of V1, while those in white show increasing expression. *p* values (corrected using a Benjamini-Hochberg False Discovery Rate procedure) for each group's significance are written in the bottom of each colored box

within a single visual area. Illustrated in Fig. 1, we used the $n = 200$ IRGs that form ascending and descending expression gradients along ventrolateral occipitotemporal cortex (Gomez et al. 2019) and measured their expression within V1 tissue samples. Linear regressions relating a given tissue sample's underlying eccentricity position with the sample's average expression of either the ascending or descending genes reveals that IRGs are not correlated with eccentricity representation in V1 ($n = 54$, R^2's < 0.003, p's > 0.7).

We next sought to further explore if a different set of genes, if any, relate to the layout of eccentricity within V1 (Fig. 2a). However, identifying genes that are correlated with the representation of the visual field within V1 is prone to false positives as a result of the inherent spatial autocorrelation that exists within gene expression (Arnatkeviciute et al. 2019). To avoid this confound, while still potentially identifying genes whose differential expression contributes to different functional portions of V1, we implemented a contrastive approach (Fig. 2b). To do so, we first binned tissue samples into separate groups with an equal number ($N = 26$) of tissue samples in posterior (0°–17° of visual space) and anterior (>17° of visual space) portions of V1. We then statistically tested if there are genes whose expression in tissue samples in the posterior portion of V1 are significantly different from those in the anterior portion. In this way, the tissue samples are contrasted and less prone to false positives compared to an approach that considers each tissue sample within a continuous map (Materials and methods). Lastly, we restrict our analysis to genes that are thought to be specifically or preferentially expressed in CNS tissue types (Materials and methods). Of the 5595 brain-related genes, we identified 152 whose expression levels were significantly different between posterior and anterior portions of V1 (Table S1).

In Fig. 2b, we plot the expression magnitude for each of the differentially-expressed genes, in each tissue sample, clustered by those that showed higher expression in either the posterior or anterior portions of V1. Sixty-three of the selected genes show an expression profile that increases from the posterior to anterior portion of V1, while the remaining 89 show the opposite pattern. These V1-related genes are almost entirely unique from the previously identified ventral visual stream genes (Gomez et al. 2019), having an overlap of only two genes. To gain a deeper understanding of the functional roles of these genes, gene symbols were submitted to an enrichment analysis resulting in five clusters of unique structural or functional properties (Fig. 2b, lower; Table S2). A raster plot shows which of the 152 genes belong to each enrichment category, and a subset of genes from each category are illustrated in the bottom of Fig. 2b. One prominent pattern that emerges is that genes encoding for inhibitory neuron populations, cation channels, as

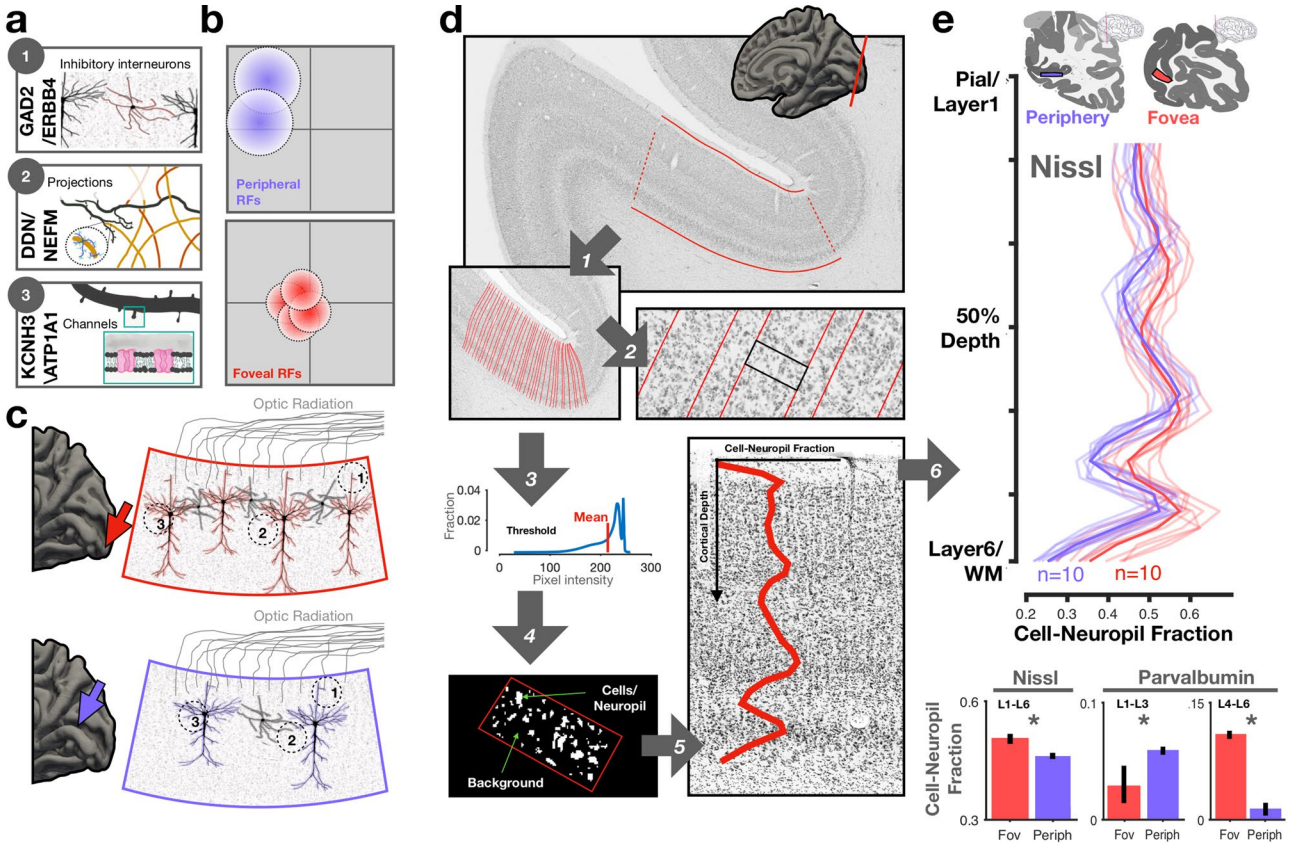

Fig. 3 Validating tissue differences between foveal and peripheral portions of human V1 predicted by a functional-genetic model. **a** Identified genes with increased expression in posterior compared to anterior portions of V1 include macromolecular tissue structures involved in inhibitory interneurons (box 1) and cell projections (box 2), suggesting higher cellular or tissue density near foveal representations in V1. Differential expression of voltage-gated receptors and ion pumps (box 3) from posterior to anterior portions of V1 mirrors functional differences between foveal and peripheral V1 receptive fields. **b** Schematic showing that receptive fields (RFs) are denser and smaller in foveal (red) compared to peripheral (purple) portions of V1. **c** A functional-genetic model resulting from **a** and **b** hypothesizes that higher RF density and increased expression of genes controlling key tissue structures will result in higher cellular/neuropil density in foveal cortex (posterior Calcarine sulcus, red arrow) compared to peripheral (anterior Calcarine sulcus, purple arrow). Right: schematic illustration of cellular/neuropil density differences between foveal (top) and peripheral (bottom) portions of V1. Colors: neurons. Gray: interneurons. Dotted circles (1–3): Where proteins of the genes in **a** are likely localized. **d** Basic steps of the BrainWalker approach developed here to quantify cytoarchitecture from coronal Nissl stains, which derives the fraction of pixels above background which we deem cell-neuropil fraction (CNF) along cortical traversals. See Materials and methods for description of the pipeline resulting in average CNF measurements across cortical layers (upper right inset) and histological slices. **e** Dark contours represent the mean (step 6). Upper insets indicate the location of the histological slices from which each ROI (colored rectangles) was defined. Red: foveal; Purple: peripheral slices of pericalcarine cortex. *Bottom, left* bar graph indicates that foveal portions have a significantly higher CNF (0.52 +/− 0.02) compared to peripheral portions (0.45 +/− 0.02) from Nissl-stained sections. *Bottom Right* Control analyses of Parvalbumin stains show that CNF varied by cortical layer indicating that foveal and peripheral cortical slices in V1 do not always vary by a global mean difference

well as cellular projections, largely decrease expression into the anterior portions of V1 that represent visual space beyond 17°. These observations, combined with modeling performed using previous measurements of the projection density of parvo- and magnocellular pathways in macaque V1 (Azzopardi et al. 1999) (Fig. S1) and denser cell and receptive-field tiling of the central visual field (Collins et al. 2010), generate a functional-genetic model (Fig. 3c) that makes the explicit prediction that cellular and tissue density should decrease as one traverses from foveal to peripheral eccentricity bands of V1.

To test this hypothesis directly, we developed a histological quantification approach (Fig. 3d), to quantify differences in cell/neuropil density between foveal and peripheral V1. Nissl-stained slices of human occipital cortex were collected from the Allen Institute, and 20 slices were chosen that were distributed along the length of the CaS. Ten were near the occipital pole to include foveal representations, while ten were taken more anterior to also include representations

of the peripheral visual field-similar to the locations of our ROIs used for the transcription analyses. To briefly describe the histological quantification pipeline (here deemed *BrainWalker;* Fig. 3d), a piece of cortical ribbon was first defined by delineating the pial and white matter borders. Traversals were then modeled across cortical layers and a sliding window was implemented between traversals. Afterwards, thresholding was applied to the local image to isolate cells and immediate structures from the background (referred to as the cell-neuropil fraction, or CNF). Finally, this CNF curve was then averaged across traversals within a slice to produce a curve that quantitatively depicts tissue density across layers in human V1. Importantly, the pixel values of tissues slices were normalized by white matter stain intensity to control for inter-slice intensity differences.

This approach reveals that the CNF of foveal tissue slices is higher than peripheral tissue slices, as shown in the CNF curves of Fig. 3e, which directly supports the prediction of the functional-genetic model. Averaging across cortical layers to produce a single CNF value for each tissue slice, we find that foveal tissue density is significantly higher than peripheral tissue [two-tailed t test, $t(18) = 2.94$, $p < 0.009$). To ensure this is not a general bias in global signal intensity resulting from the staining procedure, we repeated these analyses on tissue slices stained for interneuron protein parvalbumin (Fig. 3e, lower right; Fig. S2). While parvalbumin is expressed more highly in foveal tissue samples within cortical layers 4 through 6 [$t(8) = 5.2$, $p < 0.001$], higher expression levels are observed in the superficial layers of peripheral tissue slices [$t(8) = 2.72$, $p < 0.03$], demonstrating that higher CNF can be observed for specific protein stains in the periphery of V1. But, in general, the omnibus Nissl stain (which also stains parvalbumin-positive cells) demonstrates an overall effect of denser tissue in foveal compared to peripheral cortex, which is consistent with measurements from non-human primates (Collins et al. 2010).

Discussion

Taking advantage of the tight coupling of functional representations and cortical folding within human V1, we were able to examine the relationship between genetic transcriptions from tissue samples in V1 with map-like changes in the underlying function of each cortical sample. That is, differences in eccentricity across the cortical sheet mirror differences in the expression of two sets of genes, one in which genes are more greatly expressed in the posterior portion of V1 (0–17° of visual space) compared to the anterior portion of V1 (>17° of visual space) and another which shows the opposite pattern. Given the larger number of genes belonging to the decreasing transcription gradient, some of which result in proteins for inhibitory interneuron populations and dendritic tissues such as DDN (dendrin) and NEFH (neurofilament heavy chain), these findings predicted the existence of a tissue density gradient from posterior to anterior V1. To test this hypothesis, we developed an automated quantification pipeline for histological tissue samples that allows us to quantify tissue density across cortical layers to derive a curve of tissue density from a given region of cortex. This methodology demonstrated that the predictions made by the transcriptional observations are consistent within histological slices from foveal and peripheral portions of human V1.

Combined with previous results, the present findings demonstrate an organizational pattern in which the adult human brain employs opposed transcriptional patterns at multiple spatial scales: across the cortex (Burt et al. 2018), across areas within processing hierarchies (Gomez et al. 2019), and now within a single cortical area. Previously, we hypothesized that large-scale transcription gradients contributed to differences in population RFs across areas of the visual processing hierarchy. Here, we improve the resolution of this hypothesis by an order of magnitude to the anatomical scale of cellular structures and the functional scale of RFs within a single visual field map. Interestingly, the genes that contribute to the gradients at these different spatial scales are unique. Specifically, there was almost no overlap between the present differentially expressed V1 genes and those previously identified that contribute to the positioning of cortical areas in the visual processing hierarchy (Gomez et al. 2019). This is an important observation, as any gene that contributes to the formation of a gradient across visual regions does not necessarily contribute to a gradient that is related to a functional representation within a single visual region.

With the present multimodal approach, we were able to construct an observer-independent method for quantifying cytoarchitecture, similar to the GLI (Schleicher and Wree 1986) approach, that is importantly faster than cell counting and extracts density metrics across all layers of cortex within a defined piece of the cortical ribbon, rather than subsamples. As predicted by the transcriptional data, we observed higher cell/neuropil density in foveal compared to peripheral tissue samples. To our knowledge, this has yet to be observed and quantified in human V1, yet matches well with measurements in other species such as macaques and chimpanzees (Collins et al. 2016; Collins et al. 2010), as well as known functional gradients of striate cortex. For example, receptive field size increases from foveal to peripheral V1 (Wandell and Winawer 2015), and the ratio of neurons receiving magnocellular and parvocellular input from the LGN changes with eccentricity (Azzopardi et al. 1999), which are hallmark features of striate cortex. The disproportionate decrease in cell density of parvocellular-related neurons in macaque V1 (Azzopardi et al. 1999) would also result in overall fewer cells and interneurons, consistent with

our data (Fig. 2b, Table S2). While the receptive field of a V1 neuron is linked to geniculostriate projections (Azzopardi et al. 1999; Perkel et al. 1986), the findings from the present study also suggest that cell and tissue density differences across V1 may also play a role in RF properties, which can be further examined in future research. For example, the differential transcription of inhibitory interneuron factors between posterior and anterior portions of V1 likely contribute to differential RF properties in central and peripheral portions of V1, respectively. Additionally, temporal dynamics of receptive fields also show a gradient aligned with eccentricity representations: foveal voxels show more sustained responses to stimulus changes and peripheral voxels show a transient response pattern (Horiguchi et al. 2009; Stigliani et al. 2017). These properties align well with our observation of differential expression of several voltage-gated potassium channels between posterior (0–17° of visual space) and anterior (>17° of visual space) portions of V1. Thus, the genes identified here likely contribute to many different metabolic, structural, and functional features of human V1 with perceptual implications (Schwarzkopf et al. 2011), which complement recent work showing heritable features of striate cortex in twins (Alvarez et al. 2021; Benson, et al. 2021).

Given previous findings across species linking genetic expression to the development of functional maps within primary sensory cortices, especially V1 (Burt et al. 2018; Watakabe et al. 2007; Watakabe 2009), the present findings may seem incremental. However, we emphasize that the present findings link three lines of research. First, classic research in animals shows that gene expression contributes to the anatomical layout of V1 (Takahata et al. 2012; Yamamori and Rockland 2006) and connectivity among visual areas (Kennedy et al. 1986; Barone, Berland, Kennedy 1996; Batardiere et al. 1998). Second, previous research in animals also shows that gene expression contributes to the development of functional maps within V1 (Honig et al. 1996; Sestan et al. 2001; Syken et al. 2006). Third, modern research in humans illustrates that gene expression contributes to the arealization of the entire cerebral cortex into distinct regions (Burt et al. 2018), the organization of processing hierarchies (Gomez et al. 2019), and phylogenetic axes of macroanatomical features such as cortical thickness (Valk 2020). Here, we link these three lines of research by identifying a sparse set of genes related to the layout of the functional eccentricity map within human V1 on the two-dimensional cortical sheet. To our knowledge, these findings are the first to link the cortical layout of a functional map to a gradient of gene expression within a single cortical area of the adult human brain.

Theoretically, our present findings complement the molecular anchors hypothesis (Rosa 2002; Rosa and Tweedale 2005; Arcaro and Kastner 2015). Specifically, Rosa (2002) proposed that certain areas act as molecular anchors around which additional maps form through a self-organizing process. Specifically, in visual cortex, V1 and MT are common across primate species irrespective of whether the cortex is gyrencephalic or lissencephalic. Rosa (2002) proposed that the retinotopic representations within these regions develop early through molecular (e.g., genetic) mechanisms. Then, the cortex between V1 and MT is filled in through a self-organization process (Kohonen 1982) in which the regions adjacent to V1 and MT develop next and so forth until the cortex between these two "anchors" is completely filled in with maps. While it's likely that a unique set of genes controls these early developmental paradigms (i.e., ephrins), a similar phenomenon may explain the patterning of eccentricity map representation within adult V1 observed here. Indeed, the genes that differentiate eccentricity bands of V1 are distinct from those that differentiate V1 from MT as previously observed. Taken together, the present findings suggest that future empirical and theoretical studies considering predictions of the molecular anchors hypothesis should also consider the role of different sets of genes contributing to either (i) the formation of functional maps within human visual areas and (ii) the differentiation of a series of areas constituting the visual processing hierarchy.

In terms of weaknesses of our study, we recognize that V1 is a unique region of visual cortex, and some of the genes identified here related to eccentricity may not generalize to eccentricity representations of other portions of visual cortex or in other parts of the brain. We also recognize that cell density is often viewed as a confounding factor in transcriptomic analyses or that transcriptional differences between areas are considered a simple read-out of cell-packing density (Rakic et al. 1988). Nevertheless, we again emphasize that previous research indicates a disconnect between cyto-, myelo-, and receptor architectonic profiles of human V1 (Eickhoff et al. 2007; Amunts and Zilles 2015; Zilles and Palomero-Gallagher 2017). As such, there is not *always* a clear relationship between transcription and different functional and anatomical features of this eccentricity map in human V1. Indeed, we consider that cell density is a meaningful, as opposed to a confounding, factor–especially for human V1. Cell density has been linked to RF size in non-human primates and chimpanzees (Collins et al. 2010; Collins et al. 2016) and RF size is considered one of the basic computational units of visual processing. Additionally, previous research also shows that V1 has the highest cell density of any cortical area and that cell density decreases from early to late visual areas within the visual processing hierarchy (Collins et al. 2010). We also emphasize that (i) cell density differs among the layers of V1, (ii) the layering of V1 across species is still contentious (Balaram and Kaas 2014), and (iii) the layering of V1 is not generalizable to other primary or association areas in other lobes (Zilles and Palomero-Gallagher 2017). Thus, some of the genes identified here may

be specific to the anatomical and functional layout of human V1, which can be further examined in future research.

Finally, while transcriptional differences may contribute to the structural and functional differences across visual field maps, additional evidence suggests that such transcription shows protracted development (Gomez et al. 2019), and that RFs are even sculpted through experience and viewing behaviors (Gomez et al. 2018; Gomez et al. 2019). Thus, experience likely modulates the transcription of genes involved in structural mechanisms underlying RFs. Future work will add additional features such as connectivity (Fornito et al. 2019) and cortical layering (Watakabe et al. 2007) to the present model, which will continue to deepen our understanding of the balance between transcriptional and experiential contributions to the structure and function of human cortex. Indeed, the analysis of parvalbumin-stained slices from human V1 suggests an interaction between eccentricity and cortical layers, a prediction that can now be validated using transcriptional datasets and the *BrainWalker* software. More generally, the approach outlined here provides a tool for discovering new structural, and potentially functional, features of cortex by connecting transcription to either anatomically consistent functional representations in cortex or histologically processed tissue.

Supplementary Information The online version contains supplementary material available at https://doi.org/10.1007/s00429-021-02387-5.

Funding This work was supported by (1) start-up funds provided by the University of California, Berkeley and the Helen Wills Neuroscience Institute to KSW; (2) start-up funds provided by Princeton Neuroscience Institute to JG; and (3) The National Natural Science Foundation of China 31771251 awarded to ZZ. The funders had no role in study design, data collection and analysis, decision to publish, or preparation of the manuscript.

Data availability All analyzed data were curated from the following open datasets. Allen Human Brain Atlas (AHBA) Microarray Data: http://human.brain-map.org. Neuropythy atlas of human visual cortex: https://github.com/noahbenson/neuropythy. BrainSpan histological stains: http://www.brainspan.org/static/atlas.

Code availability Code related to processing of AHBA transcription data can be found on author ZZ's GitHub at: https://github.com/zhenzonglei/matni, and code for the beta version of BrainWalker can be found at: https://github.com/gomezj/geneccentricity.

Declarations

Conflict of interest The authors declare no conflict of interest, financial or otherwise.

References

Alvarez I, Finlayson NJ, Ei S, de Haas B, Greenwood JA, Schwarzkopf DS (2021) Heritable functional architecture in human visual cortex. NeuroImage 239:118286.

Amunts K, Zilles K (2015) Architectonic mapping of the human brain beyond brodmann. Neuron 88:1086–1107

Arcaro MJ, Kastner S (2015) Topographic organization of areas V3 and V4 and its relation to supra-areal organization of the primate visual system. Vis Neurosci 32:E014

Arnatkeviciute A, Fulcher BD, Fornito A (2019) A practical guide to linking brain-wide gene expression and neuroimaging data. Neuroimage 189:353–367

Azzopardi P, Jones KE, Cowey A (1999) Uneven mapping of magnocellular and parvocellular projections from the lateral geniculate nucleus to the striate cortex in the macaque monkey. Vision Res 39:2179–2189

Balaram P, Kaas JH (2014) Towards a unified scheme of cortical lamination for primary visual cortex across primates: insights from NeuN and VGLUT2 immunoreactivity. Front Neuroanat 8:81

Barone P, Debay C, Berland M, Kennedy H (1996) Role of directed growth and target selection in the formation of cortical pathways: prenatal development of the projection of area V2 to area V4 in the monkey. J Comp Neurol 374:1–20

Batardiere A, Barone P, Dehay C, Kennedy H (1998) Area-specific laminar distribution of cortical feedback neurons projecting to cat area 17: quantitative analysis in the adult and during ontogeny. J Comp Neurol 396:493–510

Benson NC, Winawer J (2018) Bayesian analysis of retinotopic maps. Elife 7:e40224

Benson NC et al (2021) Variability of the surface area of the V1, V2, and V3 maps in a large sample of human observers. bioRxiv 109:816

Burt JB et al (2018) Hierarchy of transcriptomic specialization across human cortex captured by structural neuroimaging topography. Nat Neurosci 93:165

Chen J, Bardes EE, Aronow BJ, Jegga AG (2009) ToppGene Suite for gene list enrichment analysis and candidate gene prioritization. Nucleic Acids Res 37:W305-311

Collins CE, Airey DC, Young NA, Leitch DB, Kaas JH (2010) Neuron densities vary across and within cortical areas in primates. Proc Natl Acad Sci U S A 107:15927–15932

Collins CE, Turner EC, Sawyer EK, Reed JL, Young NA, Flaherty DK, Kaas JH (2016) Cortical cell and neuron density estimates in one chimpanzee hemisphere. Proc Nat Acad Sci 113(3):740–745

Dale AM, Fischl B, Sereno MI (1999) Cortical surface-based analysis I. Segmentation and surface reconstruction. Neuroimage 9:179–194

Eickhoff SB, Rottschy C, Zilles K (2007) Laminar distribution and co-distribution of neurotransmitter receptors in early human visual cortex. Brain Struct Funct 212:255–267

Eickhoff SB, Yeo BTT, Genon S (2018) Imaging-based parcellations of the human brain. Nat Rev Neurosci 19:672–686

Fischl MI, Sereno AM, Dale, (1999) Cortical surface-based analysis. II: inflation, flattening, and a surface-based coordinate system. Neuroimage 9:195–207

Fornito A, Arnatkeviciute A, Fulcher BD (2019) Bridging the gap between connectome and transcriptome. Trends Cogn Sci 23:34–50

Fulcher BD (2019) Discovering conserved properties of brain organization through multimodal integration and interspecies comparison. J Exp Neurosci 13:1179069519862047

Gomez J, Natu V, Jeska B, Barnett M, Grill-Spector K (2018) Development differentially sculpts receptive fields across early and high-level human visual cortex. Nat Commun 9:788

Gomez J et al (2019) Development of population receptive fields in the lateral visual stream improves spatial coding amid stable structural-functional coupling. Neuroimage 188:59–69

Gomez J, Zhen Z, Weiner KS (2019) Human visual cortex is organized along two genetically opposed hierarchical gradients with unique developmental and evolutionary origins. PLoS Biol. 17:e3000362

Hawrylycz MJ et al (2012) An anatomically comprehensive atlas of the adult human brain transcriptome. Natures 489:391–399
Honig LS, Herrmann K, Shatz CJ (1996) Developmental changes revealed by immunohistochemical markers in human cerebral cortex. Cereb Cortex 6:794–806
Horiguchi H, Nakadomari S, Misaki M, Wandell BA (2009) Two temporal channels in human V1 identified using fMRI. Neuroimage 47:273–280
Huntenburg JM, Bazin PL, Margulies DS (2018) Large-scale gradients in human cortical organization. Trends Cogn Sci 22:21–31
Jones AR, Overly CC, Sunkin SM (2009) The Allen Brain Atlas: 5 years and beyond. Nat Rev Neurosci 10:821–828
Kennedy H, Dehay C, Bullier J (1986) Organization of the callosal connections of visual areas V1 and V2 in the macaque monkey. J Comp Neurol 247:398–415
Khrameeva E et al (2020) Single-cell-resolution transcriptome map of human, chimpanzee, bonobo, and macaque brains. Genome Res 30:776–789
Kohonen T (1982) Self-organized formation of topologically correct feature maps. Biol Cybern 43:59–69
Krienen FM, Yeo BT, Ge T, Buckner RL, Sherwood CC (2016) Transcriptional profiles of supragranular-enriched genes associate with corticocortical network architecture in the human brain. Proc Natl Acad Sci U S A 113:E469-478
Perkel DJ, Bullier J, Kennedy H (1986) Topography of the afferent connectivity of area 17 in the macaque monkey: a double-labelling study. J Comp Neurol 253:374–402
Rakic P, Goldman-Rakic PS, Gallager D (1988) Quantitative autoradiography of major neurotransmitter receptors in the monkey striate and extrastriate cortex. J Neurosci 8:3670–3690
Rosa MG (2002) Visual maps in the adult primate cerebral cortex: some implications for brain development and evolution. Braz J Med Biol Res 35:1485–1498
Rosa MG, Tweedale R (2005) Brain maps, great and small: lessons from comparative studies of primate visual cortical organization. Philos Trans R Soc Lond B Biol Sci 360:665–691
Schleicher AZ, Zilles K, Wree A (1986) A quantitative approach to cytoarchitectonics: software and hardware aspects of a system for the evaluation and analysis of structural inhomogeneities in nervous tissue. J Neurosci Methods 18:221–235
Schwarzkopf DS, Song C, Rees G (2011) The surface area of human V1 predicts the subjective experience of object size. Nat Neurosci 14:28–30
Seidlitz J et al (2020) Transcriptomic and cellular decoding of regional brain vulnerability to neurogenetic disorders. Nat Commun 11:3358
Sestan N, Rakic P, Donoghue MJ (2001) Independent parcellation of the embryonic visual cortex and thalamus revealed by combinatorial Eph/ephrin gene expression. Curr Biol 11:39–43
Smart IHM, McSherry GM (1986) Gyrus formation in the cerebral cortex of the ferret. Description of the internal histological changes. J Anat 147:27–43
Stigliani A, Jeska B, K, (2017) Grill-spector, encoding model of temporal processing in human visual cortex. Proc Nat Acad Sci 41:788
Syken J, Grandpre T, Kanold PO, Shatz CJ (2006) PirB restricts ocular-dominance plasticity in visual cortex. Science 313:1795–1800
Takahata T, Shukla R, Yamamori T, Kaas JH (2012) Differential expression patterns of striate cortex-enriched genes among Old World, New World, and prosimian primates. Cereb Cortex 22(10):2313–2321
Valk SL et al (2020) Shaping brain structure: genetic and phylogenetic axes of macroscale organization of cortical thickness. Sci Adv 6:eabb3417
Wandell BA, Winawer J (2011) Imaging retinotopic maps in the human brain. Vision Res 51:718–737
Wandell BA, Winawer J (2015) Computational neuroimaging and population receptive fields. Trends Cogn Sci 19:349–357
Watakabe A (2009) Comparative molecular neuroanatomy of mammalian neocortex: what can gene expression tell us about areas and layers? Dev Growth Differ 51:343–354
Watakabe A et al (2007) Comparative analysis of layer-specific genes in Mammalian neocortex. Cereb Cortex 17:1918–1933
Wei Y et al (2019) Genetic mapping and evolutionary analysis of human-expanded cognitive networks. Nat Commun 10:4839
Yamamori T, Rockland KS (2006) Neocortical areas, layers, connections, and gene expression. Neurosci Res 55:11–27
Zilles K, Palomero-Gallagher N (2017) Multiple transmitter receptors in regions and layers of the human cerebral cortex. Front Neuroanat 11:78